International Journal of Biological Macromolecules 160 (2020) 456–469

Contents lists available at ScienceDirect

International Journal of Biological Macromolecules

journal homepage: http://www.elsevier.com/locate/ijbiomac

Bio-based Fe_3O_4/chitosan nanocomposite sensor for response surface methodology and sensitive determination of gallic acid

Fatema Nazari, Sayed Mehdi Ghoreishi *, Asma Khoobi

Department of Analytical Chemistry, Faculty of Chemistry, University of Kashan, Kashan 87317-51167, Islamic Republic of Iran

ARTICLE INFO

Article history:
Received 24 February 2020
Received in revised form 8 May 2020
Accepted 24 May 2020
Available online 26 May 2020

Keywords:
Bio-based sensor
Fe_3O_4/chitosan nanocomposite
Gallic acid
Experimental design
Electrochemical studies

ABSTRACT

In this study, preparation of a novel bio-sensor based on Fe_3O_4/chitosan nanocomposites reported for electrochemical studies and determination of gallic acid (GA). Combination of chitosan with Fe_3O_4 nanoparticles causes to improve oxidation current of the GA. Characterization of the nanocomposite is carried out by different techniques such as X-ray diffraction, transmission electron microscopy, scanning electron microscopy, vibrating sample magnetometer, electrochemical impedance spectroscopy and cyclic voltammetry. Furthermore, multivariate optimization strategy is applied for simultaneous optimization of the chemical and instrumental parameters. Moreover, electrochemical behavior of GA at the surface of the nano-structured sensor is studied by various techniques such as chronoamperometry, chronocoulometry and linear sweep. Using these techniques, the diffusion coefficient ($D = 5.05 \times 10^{-4}$ cm^2 s^{-1} and or 4.86×10^{-4} cm^2 s^{-1}), and the kinetic parameters containing the exchanging current density ($j_0 = 0.23$ μA cm^{-2}) and electron transfer coefficient ($\alpha = 0.1$) are determined for GA, respectively. Then, the detection limit for GA is found to be 12.1 nM with a broad linear dynamic range 0.5–300.0 μM using differential pulse voltammetry DPV at the surface of the Fe_3O_4/chitosan sensor. Finally, the proposed method is successfully applied for the detection of the analyte in real samples.

1. Introduction

Gallic acid (GA; 3,4,5-triphydroxyl-benzoic acid) as a polyhydroxylphenolic compound is widely distributed in various plants, fruits and foods, where it is present either in free form or, more commonly, as an ingredient of tannins, namely gallotannin [1]. GA is very well absorbed in humans; in fact, micromolar concentrations of free and glucuronidated forms of GA and its main metabolite 4-*O*-methylgallic have been observed in human blood plasma after intake of GA-rich food. This polyphenol exhibits a variety of biochemical properties, as antioxidant, antimicrobial, and anti-inflammatory, and it has anticancer and neuro protectant effects [2]. In fact, anticancer activity of GA has been reported in various cancer cells, such as leukemia, prostate cancer [3], lung cancer, gastric, colon, breast, cervical and esophageal cancers [4]. GA find in various samples such as tea, coffee, oranges, lemons, apples, kiwi fruit, wine and vines [5–7]. Tea (Camellia), the most widely consumed drink in the world and has become an important agricultural product. The effects of lowering cholesterol, high blood pressure and depression, as well as antioxidant, antimicrobial and protect against cardiovascular disease and cancer, including the effects of tea consumption. So detection of GA with high sensitivity is necessary. So far, GA has been measured by different methods such as high performance liquid chromatography, thin layer chromatography [8], electrochemical techniques [9–12] and spectrophotometricanalysis [13]. Chromatography techniques need expensive instrumentation with high operating costs and sample preparation. However, electrochemical techniques are often favored because of their high selectivity, low cost, rapid detection and their lack of a substantial sample preparation setup. In electrochemical techniques, working electrodes play a key role in sensing applications. In recent years, using of nano-structured materials in modification of the surface of carbon paste electrodes has been development [14,15]. In this study, iron oxide nanoparticles based on chitosan (Ch) was prepared by co-precipitation method and used for modification of carbon paste electrode (CPE).The benefits such as easy synthesis, cheap raw material and also aspects of safety and toxicity caused the nanoparticles were selected. Also, for achievement the best detection limit of the analyte, Ch was used along with the nanoparticles at the surface of the modified electrode. Actually, Ch is obtained from chitin deacetylation polymer and is combination of glucosamine and *N*-acetyl glucosamine that are connected by links 1 and 4-glycoside [16,17]. Because of Ch has low conductivity and proton conductivity in acidic solutions, conductivity of the nanocomposite is improved at the surface of carbon nanotubes [18,19]. Other strategy for achieving the high sensitivity is optimization of all effective parameters on the determination of GA. Optimization by the traditional 'one-factor-at-a-time' method needs a considerable amount of experimental run, chemicals and time. An alternate strategy is a statistical

* Corresponding author.
E-mail address: s.m.ghoreishi@kashanu.ac.ir (S.M. Ghoreishi).

https://doi.org/10.1016/j.ijbiomac.2020.05.205
0141-8130/

approach, *e.g.* the response surface methodology (RSM) based on design of experiment (DOE). The RSM achieves multiple regression analysis to determine the relationship between the process variables and the response. It needs a less number of experiments in order to generate essential information for statistically acceptable results [20].

In the present work, a new nano-structured bio-sensor based on Fe_3O_4/Ch nanocomposite was prepared and used for the determination of GA. Ch in combination of Fe_3O_4 nanoparticles caused to improve oxidation current of the analyte. Other novelty of this work includes application of RSM for simultaneous optimization of all effective variables in the determination of GA. Furthermore, different parameters of GA were calculated by some electrochemical methods. Then, with regard to the performance of the nano-structured modified electrode, the nanocomposite was used for detection of GA in real samples using differential pulse voltammetry (DPV).

2. Experimental

2.1. Materials

Graphite, GA, phosphoric acid and sodium hydroxide were purchased from Merck Co. Ch with medium molecular weight and deacetylation degree of >75% was provided from Sigma-Aldrich. Also, other chemicals supplied by Sigma-Aldrich. All Chemical substances used in this study have been high purity and were used without purification. Deionized water was used in all of the experiments.

2.2. Instrumentation

To study and identification of Fe_3O_4 nanoparticles X-ray diffraction spectroscopy (XRD) (Philips, Cu K radiation ($\lambda = 1.54060$ Å), the diffraction angle (2) ranged from 10° to 80°), scanning electron microscopy (SEM) (KYKY-EM3200), transmission electron microscopy (TEM) (Philips EM208S) at an accelerating voltage of 150 kV and vibrating sample magnetometer (VSM) (laker shore 7400) were. In order to investigation of morphology of the modified and unmodified carbon paste electrodes scanning electron microscopy (SEM) and electrochemical impedance spectroscopy (EIS) PGSTAT 35 (Eco chemie Utrecht, Netherlands) were applied. Electrochemical measurements were performed by a Sama 500 potentiostat (Isfahan, Iran). All experiments were performed using a conventional three-electrode electrochemical cell composed of a platinum wire (Metrohm, Switzerland), an unmodified or modified carbon paste electrode (2 mm in diameter) and an Ag/AgCl/KCl 3.0 M electrode (Metrohm, Switzerland), as an counter, working and reference electrodes, respectively. A Metrohm 691 pH meter was applied for preparing the phosphate buffer samples with different pHs. An ultrasound bath (BandelinSonorex, Germany) operated at constant frequency of 35 kHz was used for dispersing of nanopowders.

2.3. Synthesis of Fe_3O_4 nanoparticles

In this research the co-precipitation method was used to prepare Fe_3O_4 nanoparticles. In this method, $Fe^{2+}$and Fe^{3+} ions are mixed together with a ratio of 1 to 2. For this purpose, the amount of 1.15 g of $FeCl_2 \cdot 4H_2O$ and 3.0 g $FeCl_3 \cdot 6H_2O$ individually were prepared in deionized water and then the solutions were mixed. In order to remove oxygen, N_2 gas into the flask at room temperature was placed in an ultrasonic bath. Then, 20 mL ammonia was added to the flask for 15 min and put under ultrasound. Then, the mixture was precipitated by a strong magnet and the precipitate was washed with deionized water and ethanol. The precipitate was obtained after drying in the oven at 45 °C for 30 h.

2.4. Preparation of the modified electrode

To reach the proper amounts of nano-particles and chitosan, the optimization step were performed and reached to the optimum value for each substance. After that for preparation of the modified electrode, 0.0820 g Fe_3O_4 nanoparticles were dispersed with 2 mL deionized water in an ultrasonic bath (power: 200 W) for 45 min. Next, 0.4900 g graphite powder and 0.015 g Ch were mixed with the above dispersant. After drying, 0.18 g paraffin oil was added, well mixed and then transferred to a polyethylene tube. Finally, a copper wire was inserted to the electrode to create an electrical contact. Also, before each experiment, the electrode surface was polished with weighing paper.

2.5. Optimization strategy

The optimization of all effective parameters on the DPV responses of GA was performed using RSM which is a collection of statistical and mathematical methods that are suitable for analysis and modelling of problems when a response is influenced by several variables. However, before RSM a DOE is needed. Rotatable central composite design (RCCD) is a useful method for experimental design that is combined with RSM to analyse the interaction between the variables with a minimum number of experiments. This design contains of three parts: (1) a full factorial or fractional factorial design; (2) an additional design, often a star design in which experimental points are at a distance α from its centre; and (3) a central point. RCCD present the following characteristics: (1) require an experiment number according to $N = 2f + 2f + r$, where f is the number of factors and r is the replicate number of the central point; (2) α-values depend on the number of factors and can be calculated by $\alpha = \pm 2^{f/4}$; (3) all factors are studied in five levels. The response behavior is related to the selected independent variables by a second-order polynomial. The generalized response surface model is shown by Eq. (1) [20]:

$$Y = \beta_0 + \sum_{i=1}^{4} \beta_i X_i + \sum_{i=1}^{4} \beta_{ii} X_i^2 + \sum \sum_{i<j=1}^{4} \beta_{ij} X_i X_j \quad (1)$$

where Y describes the predicted response, X_i is the independent factor, β_0 is intercept, β_i, β_{ii} and β_{ij} are the linear, quadratic and interaction coefficients, respectively.

In the present study, RCCD was used for investigation of four effective factors on the DPV response of GA. The factors contain pH, iron oxide/chitosan amount, scan rate and pulse height. Also, MINITAB® Release 16, developed by Minitab Inc. (USA), a statistical software package, was applied for data processing and studying linear terms, squared terms and interaction between the factors. The significance level 95% was selected for the mathematical model and surface response.

2.6. Real samples preparation

Determination of the GA in real sample is one of the main purposes of the proposed electrode. The ability was checked by the detection of GA in green tea which is contains GA. In order to prepare the sample, 2.0 g powder of green tea leaf was transferred in a mortar. Then, 0.5 mL of nitric acid was added and the solution was heated to drying point. Then, deionized water was added to the dry material. After dissolving, the solution was filtered and diluted to 100.0. Finally, 2.0 mL of the sample was transferred into the electrochemical cell containing phosphate buffer pH = 2.0 for detection of GA using DPV.

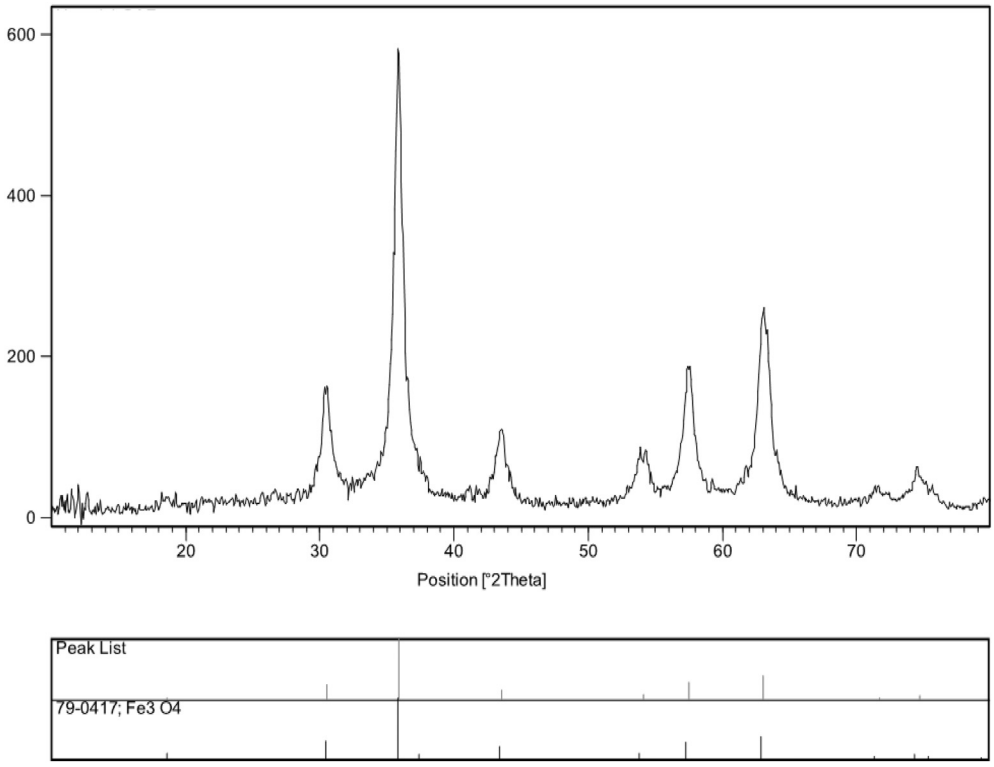

Fig. 1. XRD pattern of the Fe_3O_4 nanoparticles.

3. Results and discussion

3.1. Structural and morphological studies of the nano-structured materials

3.1.1. XRD spectra

In order to study the structure of iron oxide nanoparticles, XRD was applied. X-ray diffraction pattern of the sample can be seen in Fig. 1. The XRD pattern of the Fe_3O_4 nanoparticles presents several diffraction peaks, which are placed at Bragg angle values of at 30.42, 36.01, 43.58, 54.46, 57.69, 63.01, 71.96 and 74. 58. Using the data, average crystalline size of the iron oxide nanoparticles was calculated based on the Scherrer equation about 45 nm.

3.1.2. TEM and SEM analysis of the Fe_3O_4 nanoparticles

For study of the size and morphology of iron oxide nanoparticles microscopic techniques were used. In Fig. 2 TEM [21] and SEM images of the nanoparticles are shown. According to the Fig. 2, the average particle size of the iron oxide nanoparticles was obtained 52 nm. The TEM image shows magnetic Fe_3O_4 nanoparticles are almost spherical or ellipsoidal.

3.1.3. VSM analysis of the Fe_3O_4 nanoparticles

The magnetic properties of Fe_3O_4 nanoparticles were studied by VSM to confirm superparamagnetic properties of the nanoparticles.

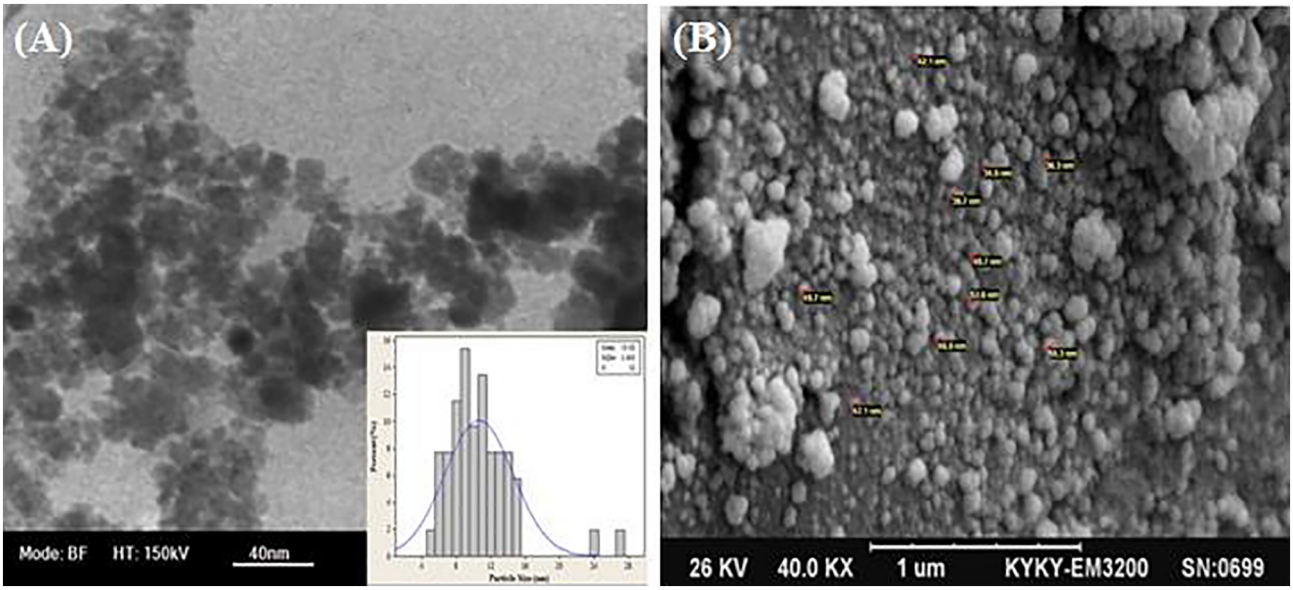

Fig. 2. TEM (A) and SEM (B) micrographs of Fe_3O_4 nanopowders.

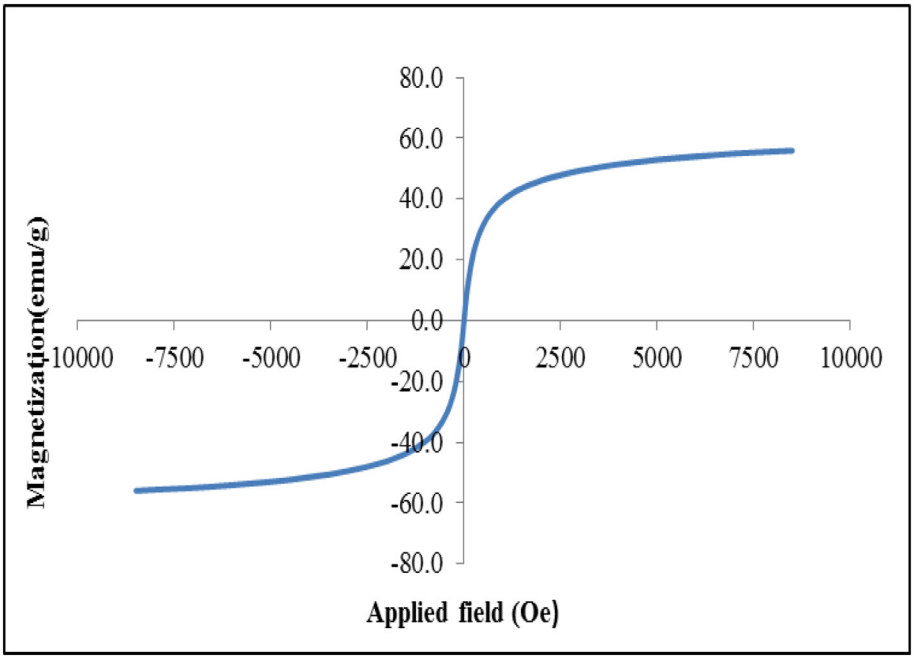

Fig. 3. Magnetization hysteresis loops of Fe_3O_4 nanoparticles.

Magnetization hysteresis loops at 25 °C of Fe_3O_4 nanoparticles are shown in Fig. 3. The nanoparticles showed no magnetic hysteresis and presented superparamagnetic property. This property prevents nanoparticles from magnetically aggregation in the absence of magnetic field and then, nanoparticles can re-disperse rapidly when the magnetic field is switched off.

3.1.4. SEM analysis of the nanocomposite modified electrode

The Fe_3O_4/chitosan/carbon paste electrode (Fe_3O_4/Ch/CPE) was first characterized by SEM. Fig. 4 presents the SEM images of CPE (a), Fe_3O_4/CPE (b), Ch/CPE (c) and Fe_3O_4/Ch/CPE (d). As can be observed the presence of Fe_3O_4 and Ch at the surface of the modified electrodes is very clear.

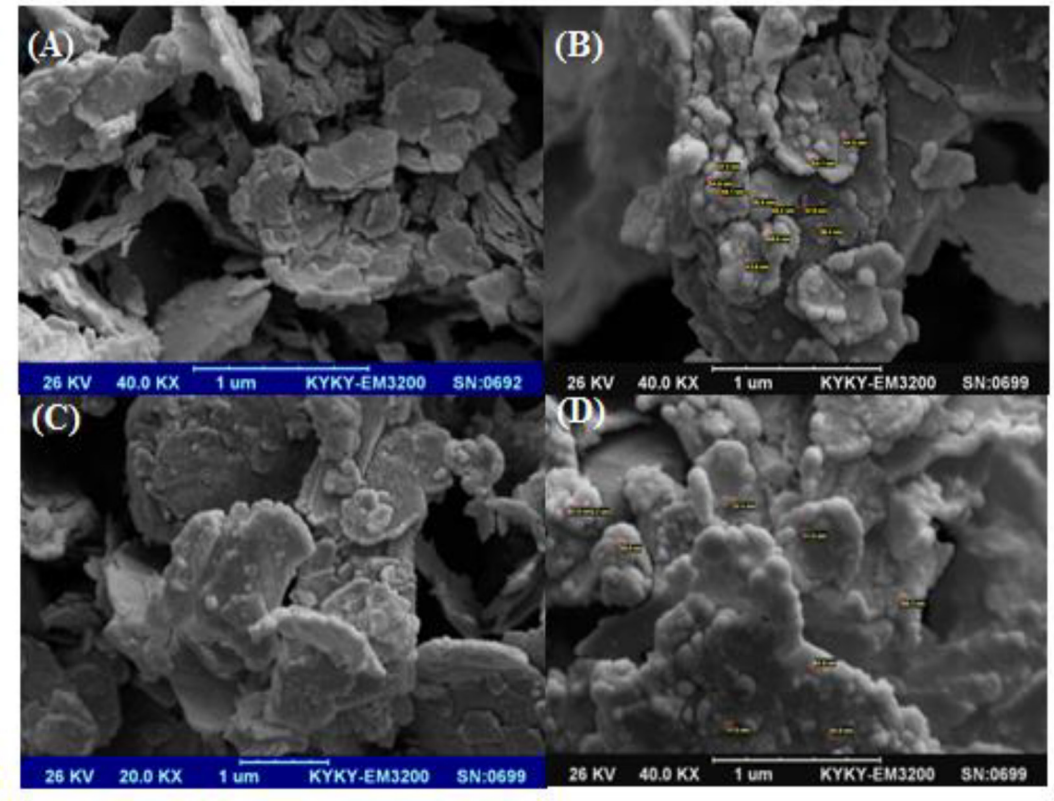

Fig. 4. SEM images of (A) unmodified CPE and (B), (C), (D) modified electrode by Fe_3O_4 nanoparticles, chitosan, Fe_3O_4/Ch, respectively.

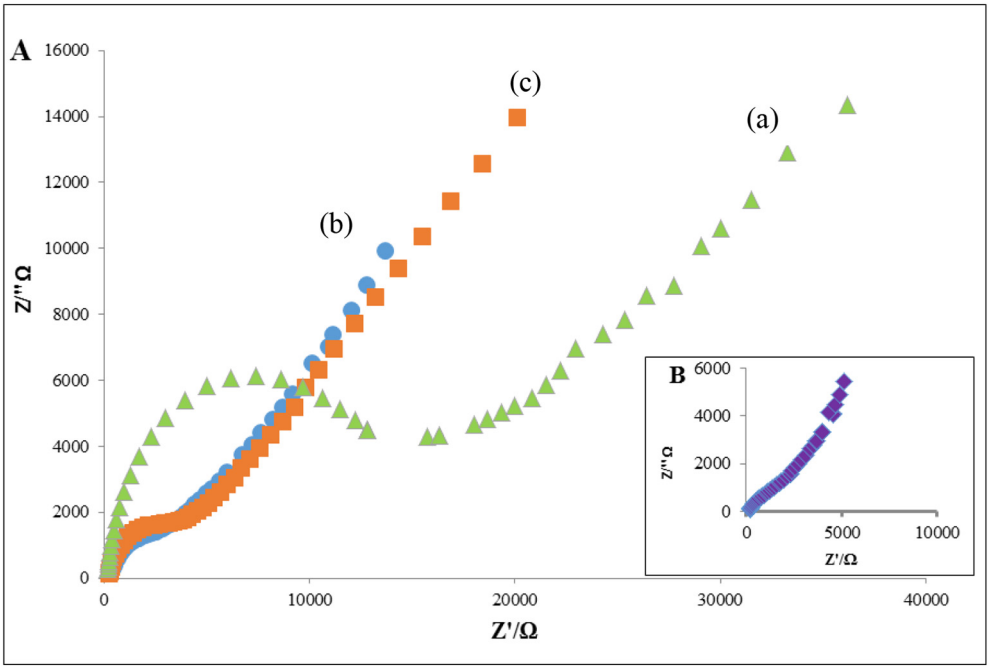

Fig. 5. (A) Nayquest curves: (a) unmodified electrode and (b), (c) modified electrode by Fe_3O_4 nanoparticles, chitosan, respectively (B) Nyquist curves of Fe_3O_4/Ch/CPE.

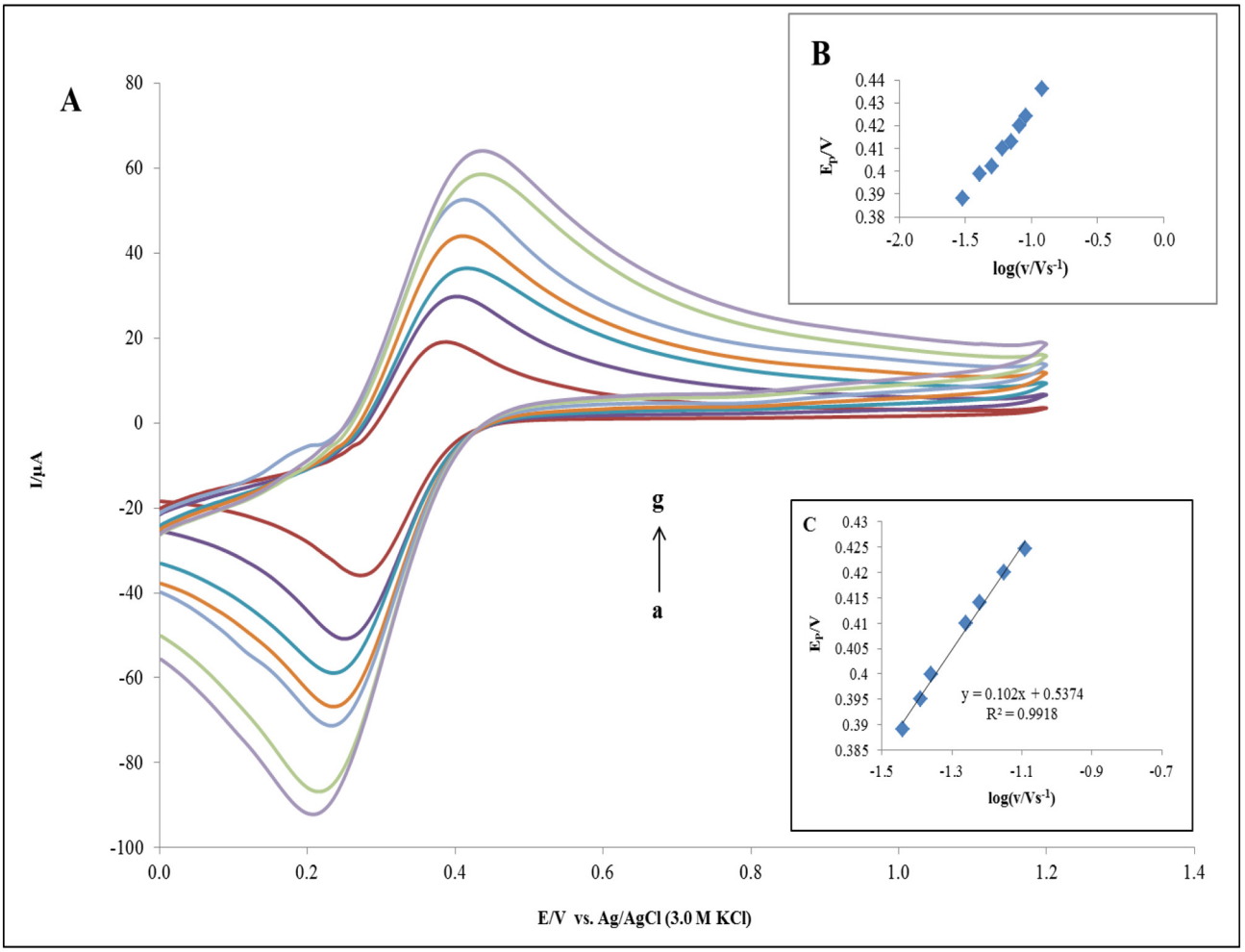

Fig. 6. (A) Cyclic voltammograms of phosphate buffer (pH = 2.0) containing 5.0 mM $[Fe(CN)_6]^{-4}$ using various scan rates 30.0, 40.0, 50.0, 60.0, 70.0, 80.0 and 90.0 mV s^{-1} (a to g), (B) ΔEp *vs.* log (ν/V s^{-1}) and (C) as (B)in high scan rates.

3.1.5. Characterization of the nanostructured modified electrode by EIS

In the present study, EIS was also used to characterize the electrodes. Fig. 5(A) shows impedance spectrum of the bare (a), Fe_3O_4/CPE (b), Ch/CPE (c) and Ch/Fe_3O_4/CPE (Fig. 5(B)) in the presence of 5.0×10^{-3} M $K_4Fe(CN)_6$ and $K_3Fe(CN)_6$ solution in 0.2 M phosphate buffer (pH 2.0) as a probe sample. Using the analysis, electron transfer resistance (R_{ct}) can be calculated to feature conductivity and dielectric intermediate electrode/electrolyte properties. According to the Fig. 5, the R_{ct} values for the bare CPE, Fe_3O_4/CPE, Ch/CPE and Ch/Fe_3O_4/CPE were obtained 12,730, 2924, 2077 and 1178 Ω, respectively. The decrease in R_{ct} can be attributed to the presence of the Fe_3O_4 and Ch at the CPE that accelerates the transfer of the electrons at the surface of the electrode.

3.1.6. Voltammetric study of Fe_3O_4/Ch/CPE

For more study of the behavior of Fe_3O_4/Ch nanocomposite at the surface of the modified electrode Fe^{2+}/Fe^{3+} probe solution was used. Fig. 6(A) displays the spectra of the modified electrode in the presence of 5.0×10^{-3} M $[Fe(CN)_6]^{3-/4-}$ in 0.2 M phosphate buffer (pH 2.0) by cyclic voltammetry (CV). Fig. 6(B) shows the variations of peak potentials (E_p) as a function of logarithm of the potential scan rate. By the studies, electron transfer rate constant (K_S, S^{-1}) and charge transfer coefficient (α) between the probe and Fe_3O_4/Ch/CPE were calculated using Laviron equation (Eq. (2)) [22]. Thus, value of the α and the K_s was obtained 2.08 and s^{-1} 0.458, respectively.

$$\text{Log } k_s = \alpha \ \log(1-\alpha) + (1-\alpha)\log\alpha - \log(RT/nFv) - \alpha(1-\alpha)\, n_\alpha\, F\Delta E_p/2.3RT \quad (2)$$

3.2. Electrochemical studies of GA

3.2.1. Multivariate optimization studies

In the preset work, RCCD and RSM methods were used for the design of experiments and multivariate optimization, respectively. The effects of the different parameters on the responses of GA were investigated through these methods. Chemical factors contain pH (A) and iron oxide nanoparticles and chitosan (B) and also, instrumental factors contain scan rate (C) and pulse height (D). The selected range for the factors is 1.5 to 3.5, 30% to 70%, 0.01–0.13 V s^{-1}, and 0.02–0.1 V, respectively (Table.1). In this design, the number of factors is 4, and considering the 3-point iteration, the total number of tests contains 27 tests. For this purpose, the design of experiments was performed using Minitab software. Then, the differential pulse voltammograms of each test for GA were recorded at the surface of Fe_3O_4/Ch/CPE. Also, using the 27 tests, an appropriate model was selected. Next, the results were analyzed and reported in Table 2. According to the Table 2, the *P*-value of lack of fit (LoF) was 0.47 indicating insignificant LoF for the selected model. Also, R-squared and Adjusted R-Squared values were 97.48% and 93.96%, respectively, which indicate the validation of the model. Finally, the optimum amount of each effective factor was obtained. The actual optimized values are reported in Table 3. Also, optimum values by graphical analysis using Minitab software as an optimal response curves, surface plots and contour plots were extracted (Figs. 7, 8). Furthermore, some experimental runs were performed Based on the optimal conditions. The results are presented in Table 4 and approve that the obtained peak current has good agreement with the predicted value by the mathematical model.

Table 2
Analysis of variances for GA using RSM.

Source	Degree of freedom	Sum of squares	Mean square	F value	*P* value
Regression	14	168.35	12.02	27.66	<0.0001
Linear	4	106.02	26.73	61.49	<0.0001
A	1	73.96	73.96	170.13	<0.0001
B	1	0.029	0.029	0.07	<0.0001
C	1	6.79	6.79	15.64	<0.0001
D	1	26.13	26.13	60.12	<0.0001
Square	4	48.38	12.09	27.82	<0.0001
A^2	1	0.24	4.58	10.53	<0.0001
B^2	1	21.09	31.17	71.71	<0.0001
C^2	1	18.85	16.04	36.91	<0.0001
D2	1	8.20	8.20	18.86	<0.0001
Interaction	6	13.056	2.1760	5.01	0.013
AB	1	0.117	0.117	0.27	0.615
AC	1	1.562	1.562	3.59	0.087
AD	1	9.786	9.786	22.51	0.001
BC	1	0.287	0.287	0.66	0.435
BD	1	0.488	0.488	1.12	0.314
CD	1	0.815	0.815	1.88	0.201
Residual	10	4.347	4.347	–	–
Lack of fit	8	3.708	0.4636	1.45	0.470
Pure error	2	0.639	0.3194	–	–
Total	24	172.704	–	–	–
R-squared = 97.48%		Adj. R-squared = 93.96%			

3.2.2. Electrochemical behavior of GA at the modified electrode

To understand the catalytic activity of the nano-structured modified electrode, CV was investigated in the presence of 100.0 μM GA in 0.2 M phosphate buffer (pH = 2.0) in scanning rate of 130.0 mV s^{-1} (Fig. 9). Based on the Fig. 9, the produced current by GA on the Fe_3O_4/CPE and Ch/CPE are 1.5 and 2 times more than the unmodified electrode, respectively. However, when CPE was modified by Fe_3O_4/Ch nanocomposite increased the current of GA about 2.5 times. This result demonstrates of the sensitivity of the Fe_3O_4/Ch/CPE.

3.2.3. Influence of scan rate

Fig. 10(A) shows cyclic voltammograms of GA in different scanning rates at the surface of Fe_3O_4/Ch/CPE. According to the Fig. 10(B) the GA oxidation process was controlled by mass transfer according to Eq. (3) [22]:

$$I_{pa} = 2.99 \times 10^5\, n\, [(1-\alpha)\, n_\alpha]^{1/2}\, A\, D^{1/2}\, C\, \upsilon \quad (3)$$

In the Eq. (3), n is the number of electrons involved in the redox reaction, A (cm^2) is the electrode surface area, C (mol cm^{-3}) is the GA concentration and D (cm^2 s^{-1}) is the diffusion coefficient. Using the

Table 1
Coded and actual levels of effective factors for GA.

Factors		Coded levels				
Name		−2	−1	0	+1	+2
X_1	pH	1.5	2.0	2.5	3.0	3.5
X_2	Fe_3O_4/Ch%	30%	40%	50%	60%	70%
X_3	Scan rate (v s^{-1})	0.01	0.04	0.07	0.1	0.13
X_4	Pulse height (v)	0.02	0.04	0.06	0.08	0.1

Table 3
Optimized conditions for GA using RSM.

Factors		The coded optimized values	The actual optimized values
X_1 (A)	pH	−2	1.5
X_2 (B)	Fe_3O_4/Ch%	−0.14	48.74
X_3 (C)	Scan rate (V s^{-1})	0.78	0.1
X_4 (D)	Pulse height (V)	−1.27	0.044

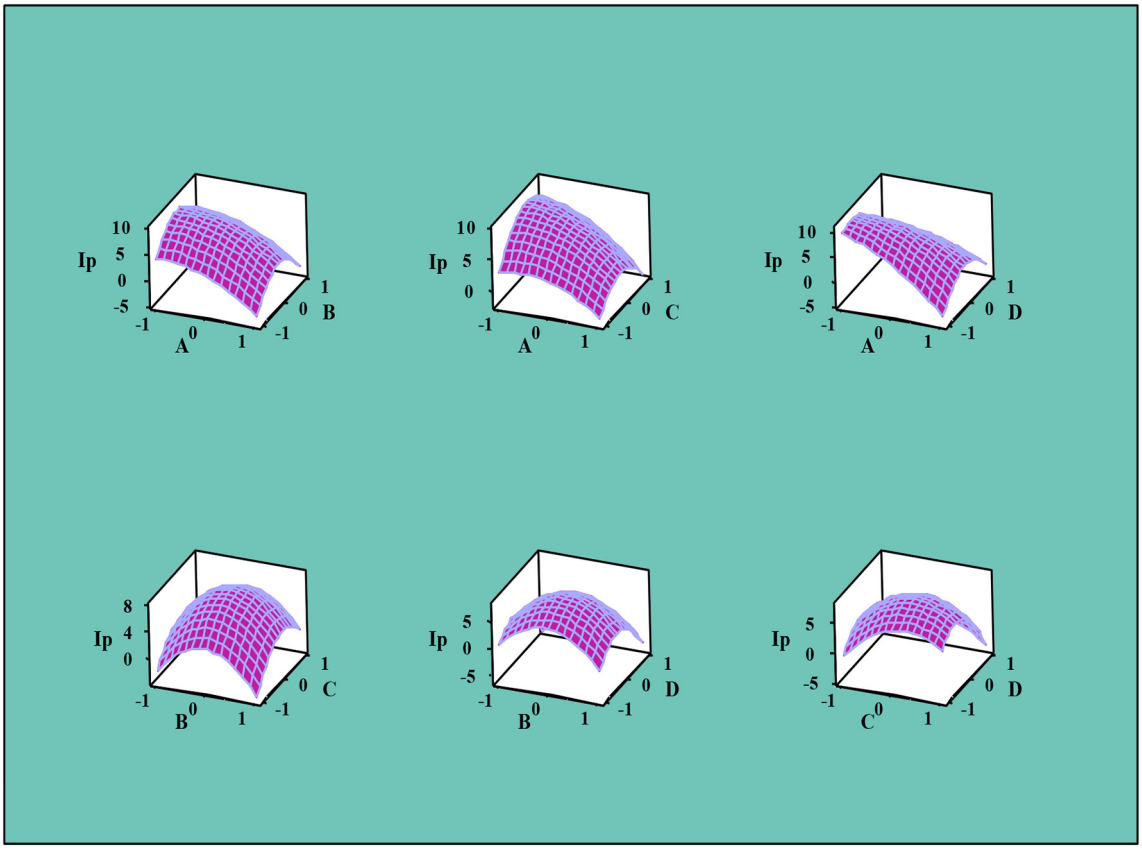

Fig. 7. Surface plot of GA at the Fe_3O_4/Ch/CPE.

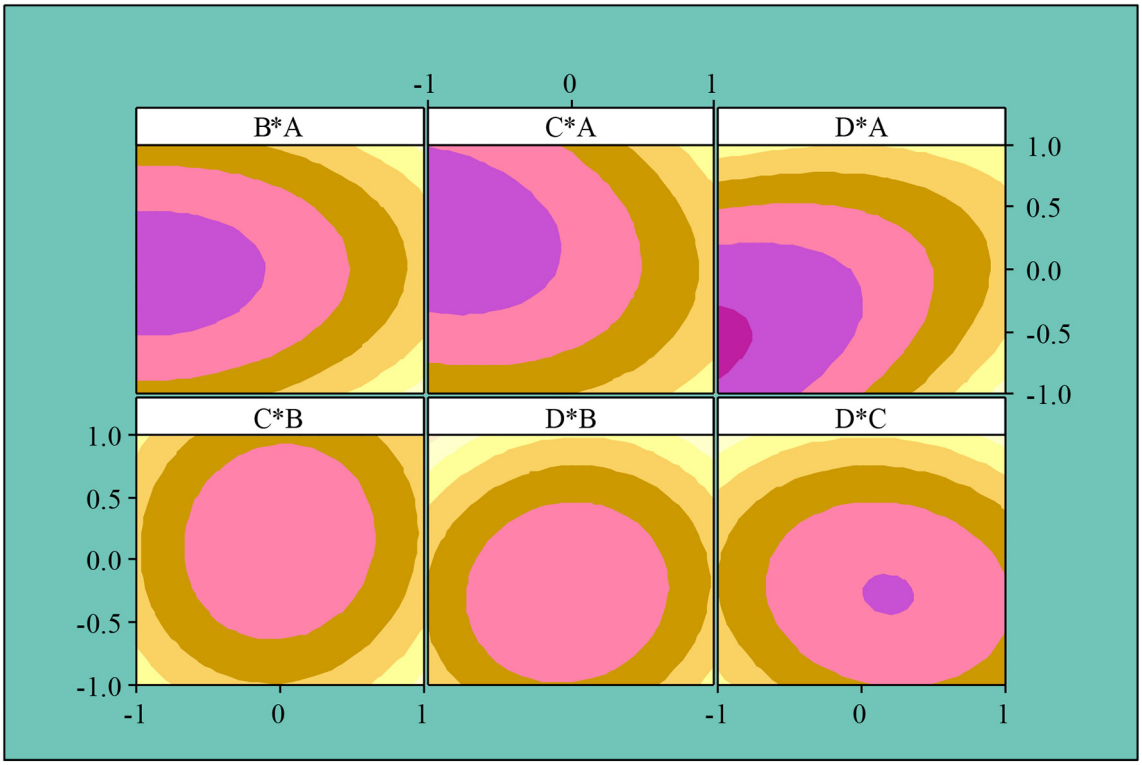

Fig. 8. Contour plot of GA at the Fe_3O_4/Ch/CPE.

Table 4
Results of the experimental runs compared with the predicted values by the mathematical model.

Parameters	Predicted response (Ave.)	95% CI low·high	Predicted Std. Dev.	Observed response ($n = 3$)
Obtained values	8.72	8.12–8.85	0.19	8.51 ± 0.12

Fig. 10 by increasing in the scan rate from 10.0–130.0 mV s^{-1} an increasing in the current of GA is happened.

3.2.4. pH dependence study

Using DPV the effects of pH values in the determination of GA at the modified electrode was studied. DPV graphs of GA at the surface of the modified electrode were studied in phosphate buffer in the range of pH of 2.0 to 6.0. Fig. 11 shows by increasing in the pHs an shift in potential to negative values is observed. This movement indicates that the proton was involved in oxidation process of GA. Also, these potentials values have liner relationship with pHs as follow equation:

$$E_p\ (V) = -0.067\ pH + 0.602\ \left(R^2 = 0.9905\right)$$

Using the Nernest equation the amount of 1.8 is obtained for number of the protons. Thus, it can be stated that the number of two-electron oxidation and two protons exchanged in the reaction. So, possible mechanism for oxidation of GA can be shown in Scheme 1 [24].

3.2.5. Chronoamperometry and chronocoulometry studies

To determination of diffusion coefficient (D) of GA, chronoamperometry (CHA) technique was performed. Fig. 12 displays chronoamperograms of GA in 2.0 M phosphate buffer (pH = 2.0) at different concentrations. As can be observed with increasing of the concentrations of GA, anodic current is increased in step primary potential. By the slope resulting from Fig. 12 and Cottrell equation (Eq. (4)) the value of D was calculated to be 5.05×10^{-4} cm^2 s^{-1}.

$$I = nFAD^{1/2}C\pi^{-1/2}t^{-1/2} \quad (4)$$

In order to supporting the data that was obtained from CHA technique, the diffusion coefficient (D) of GA was also calculated using chronocoulometry (CHC). Fig. 13(A) shows chronocoulograms of GA in phosphate buffer (pH 2.0) for various concentrations of the analyte at the modified electrode with step potential of 1000.0 mV. Using the data the value of D was obtained near the CHA technique (4.86×10^{-4} cm^2 s^{-1}).

3.2.6. Linear sweep voltammetry study

Linear sweep voltammetry (LSV) and Tafel plot was performed to determination of the kinetic parameters of GA such as exchange current (j_0) and transfer coefficient (α). Thus, the linear sweep voltammograms of GA in 0.2 M phosphate buffer (pH = 2.0) were recorded (Fig. 14(A), scan rate: 130.0 mV s^{-1}). So, by slope and intercept of the Tafel curve (Fig. 14(B), i_0 and α were obtained, respectively. Using the average of the data, i_0 and α for GA were calculated 0.23 μA cm^{-2} and 0.1, respectively.

3.2.7. Calibration curve and detection limit

To determine of the detection limit, differential pulse voltammograms of GA in the optimum conditions was drawn at the surface of Fe_3O_4/Ch/CPE (Fig. 15 (A)). Also, Based on the Fig. 15(B) a liner relationship between GA and peak current is observed with the linear regression equation of $Y = 0.0232x + 0.1749$ ($R^2 = 0.984$). Moreover, the relative standard deviation (RSD) of the buffer (blank) for fifteen determinations was calculated. Using Eq. (5), where S_b and m are the standard deviation of the blank solution and the slope of the calibration curve, respectively, the detection limit for GA was calculated to be

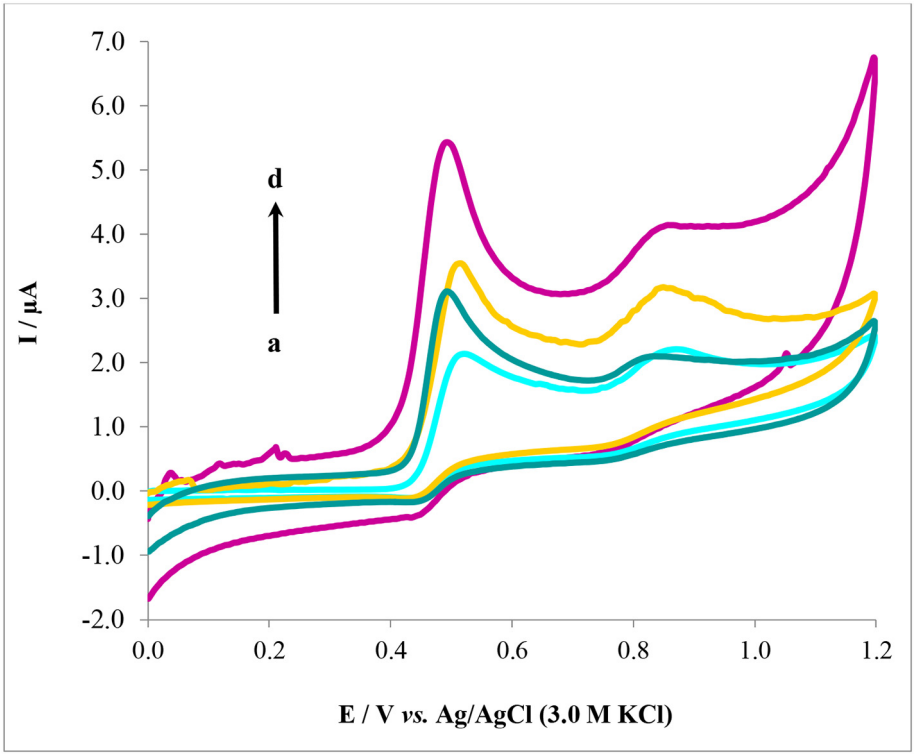

Fig. 9. Cyclic voltammograms of phosphate buffer (pH 2.0), in the presence of 100.0 μM GA by CPE (a), Fe_3O_4/CPE (b), Ch/CPE (c), Fe_3O_4/Ch/CPE (d).

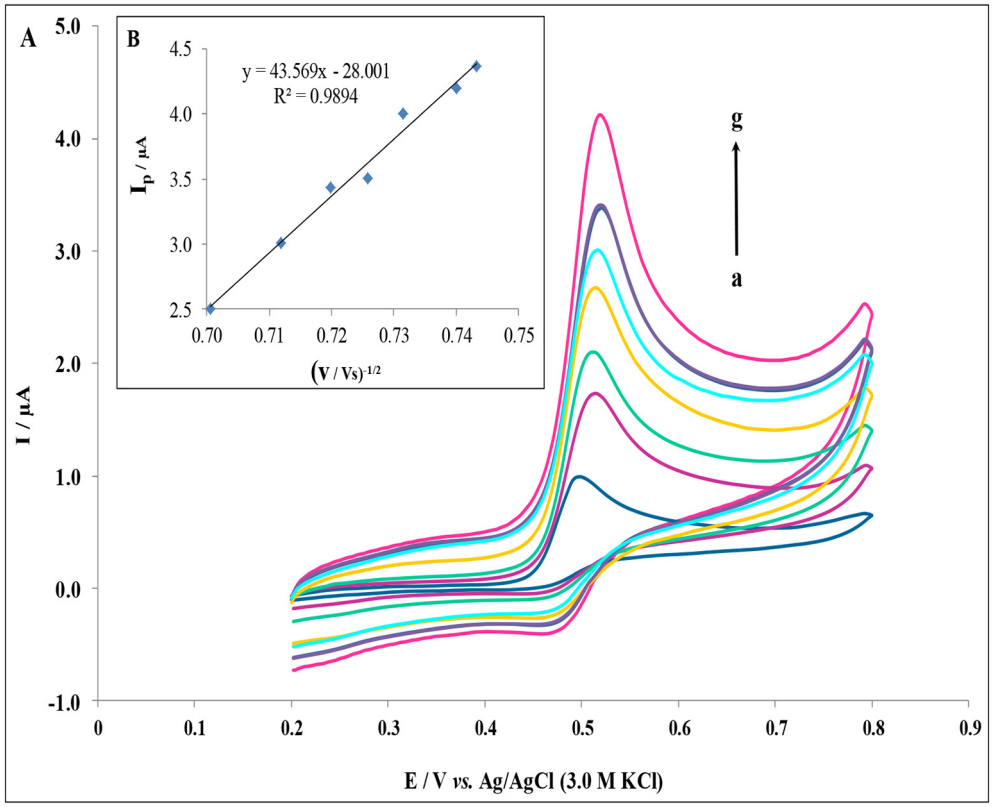

Fig. 10. Cyclic voltammograms of Fe_3O_4/Ch/CPE in phosphate buffer (pH 2.0) for 50.0 µM SA, using various scan rates: 10.0, 20.0, 30.0, 40.0, 50.0, 60.0, 70.0, 80.0 and 90.0 mV s^{-1} (a to j), (A) Current *vs.* E (mV), (B) Peak current *vs.* $v^{1/2}$.

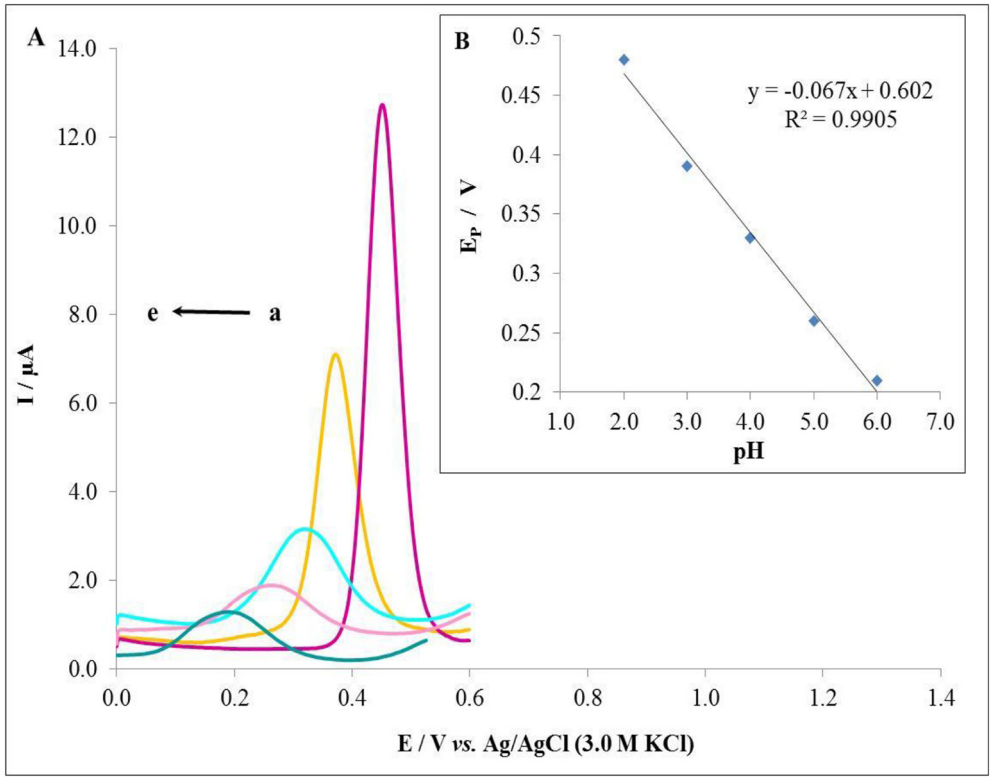

Fig. 11. (A) DPV of a solution containing 100.0 µM GA at various pH values, at Fe_3O_4/Ch/CPE, (B) dependency graph of GA oxidation pick to pH solutions at scan rate 130 mV s^{-1}.

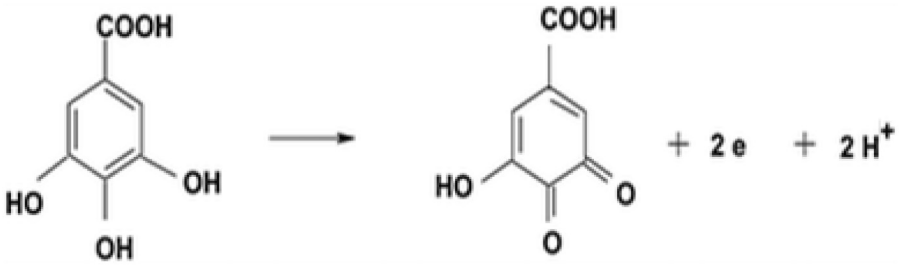

Scheme 1. Mechanism of GA oxidation.

12.1 nM. Using the study, linear calibration range for GA was obtained in the range of 0.5–300.0 μM. The results are superior to the values reported by other research groups (Table 5) [23–28].

$$c = 3\,S_b/m \tag{5}$$

3.2.8. Repeatability and stability of the nanostructured modified electrode

To investigate of the repeatability of the modified electrode, the five electrode was prepared and five differential pulse voltammogram of each electrode were recorded in phosphate buffer with pH = 2.0 for 100.0 μM of GA in the optimal conditions. The DPV responses of the electrodes were compared and the RSD was calculated to be 2.7% that suggest the highly repeatable surface for the proposed modified electrode.

The stability of the modified electrode in standard solution with a concentration of 100.0 μM GA in the phosphate buffer (pH = 2.0) was investigated for a 2-week period (with three replicates in each day and an average standard deviation value of 2.9%) at the surface of the modified electrode and DPV. Fig. 16 shows the electrode response decreases only 2.38% rather than its initial value. Based on the studies the results show Fe_3O_4/Ch/CPE has a good long-time repeatability and stability for the determination of GA.

3.2.9. Interference studies

To investigating the effects of various compounds interferences in the determination of GA, the DPV was applied. For the study, the peak current of 100.0 μM of GA in 0.2 M phosphate buffer with pH = 2.0 was determined. This study was repeated for 5 times and the average and standard deviation was calculated. Next, GA with 200 times in the

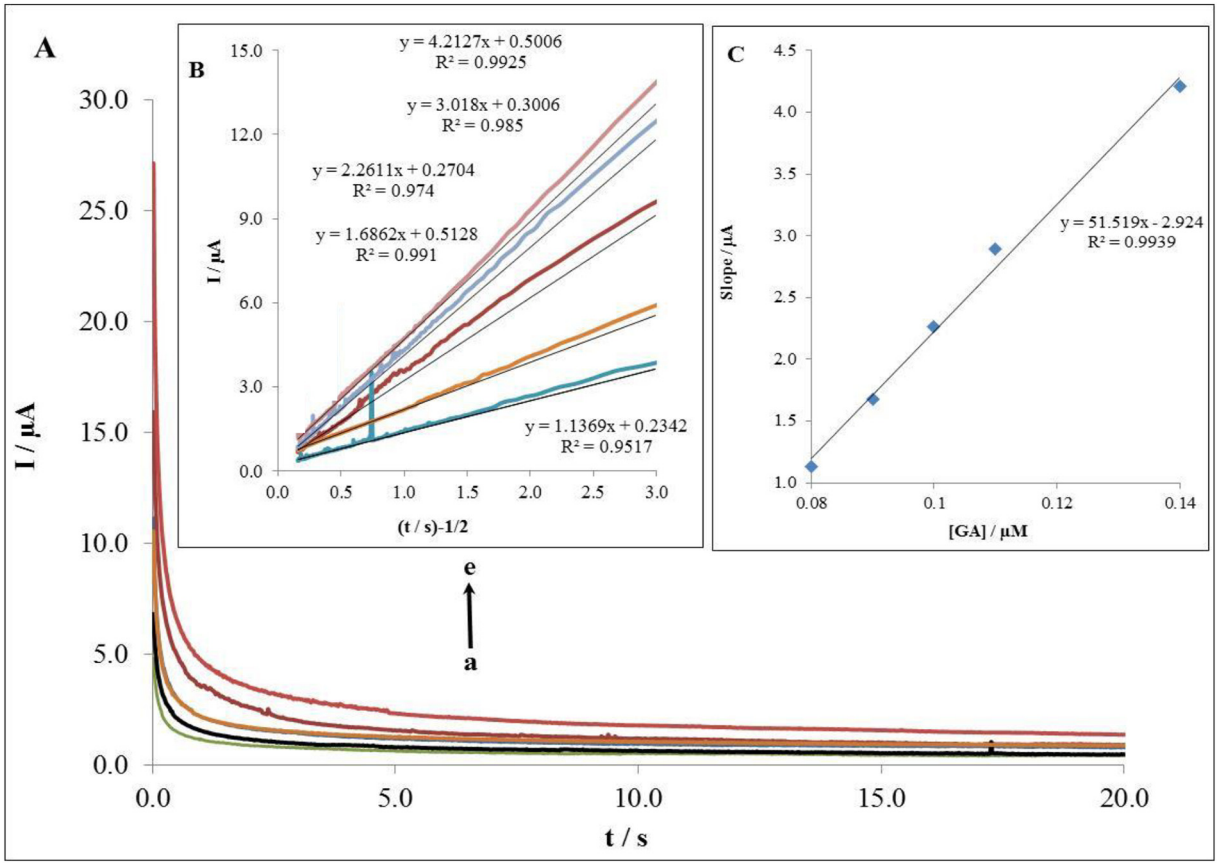

Fig. 12. Chronoamperograms obtained at the Fe_3O_4/Ch/CPE in phosphate buffer (pH = 2.0) for various concentrations of GA with potential step of 1000.0 mV. a to e correspond to 0.47, 0.56, 0.78, 0.97 and 1.15 μM of GA (A); Plots of I *vs.* $t^{-1/2}$ ($s^{-1/2}$) obtained from chronoamprograms a–e (B), A plot of the slope of the straight lines *versus* the concentration of GA (C).

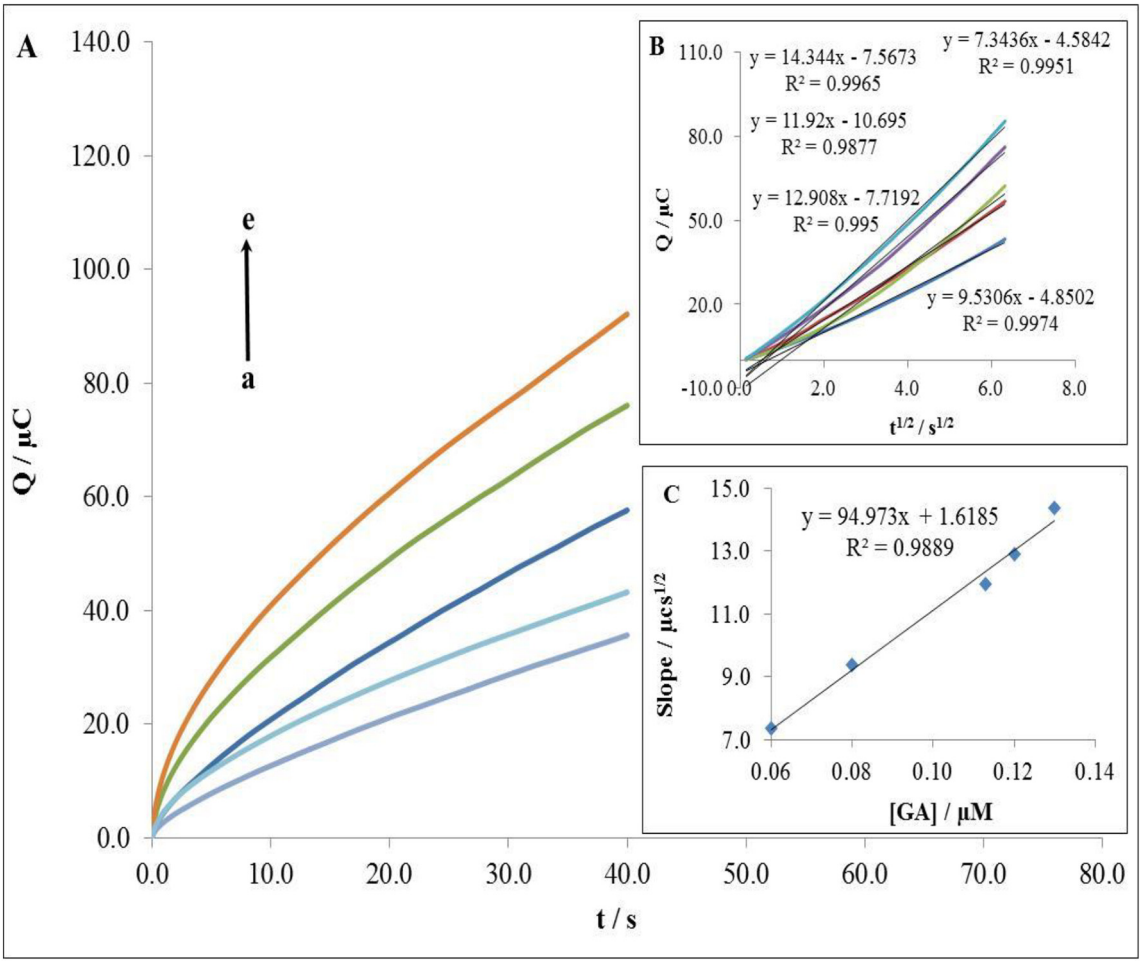

Fig. 13. (A) Chronocoulograms of phosphate buffer (pH = 2.0) for various concentrations of GA at the modified electrode, potential step of 1000.0 mV. a to e correspond to 20.0, 30.0, 40.0, 50.0, 60.0 and 70.0 µM of GA, (B) Plots of Q *vs.* $t^{-1/2}$ ($s^{-1/2}$) and (C) Plot of the slope of the straight lines *versus* the concentration of GA.

concentration was measured in the presence of the interfering substance. According the investigation amount of the differences of GA in the absence and presence of interfering substances were <5%. Table 6 shows the effect of the interfering substances in determination of GA at the surface of Fe_3O_4/Ch/CPE.

3.2.10. Real samples analysis

The ability of the proposed procedure for detection of GA was also studied in real samples. For this purpose, green tea leaf that contains GA, as a real sample was selected. Tea samples were determined by a standard addition method to keep any matrix effect. For preparation of the sample, green tea powder was dissolved in nitric acid on the heater till solution to dry. The rest of the substance was dissolved to 100 mL and take 2.0 mL to electrochemical cell. The standard addition method was performed for testing recovery by three repeatable measurements on each sample. The results are listed in Table 7. The recovery rates of the spiked samples are acceptable, indicating that the sample matrix does not interfere with the detection procedures.

4. Conclusions

This study tried to investigate the electrochemical behavior of a bio-based Fe_3O_4/Ch nanocomposite sensor. At first, co-precipitation method was used for synthesis of Fe_3O_4 nanoparticles. Then, Ch was combined with Fe_3O_4 nanoparticles to prepare a bio-based nano-structured modified electrode. The characterization of the bio-based nanocomposite was studied by different techniques such as XRD, TEM, SEM, VSM, EIS and CV. The modified sensor was improved oxidation peak current of GA, indicating that the modified electrode has a great electrocatalytic activity for GA. Also, different techniques such as CHA, CHC and LSV were applied for investigation of the electrochemical behavior of GA at the surface of the modified electrode. After optimizing the experimental conditions using multivariate optimization strategy, the anodic peak current of GA showed a linear correlation to its concentration in a broad linear dynamic range with low detection limit. Also, the proposed method creates a sensitive and selective approach for the detection of GA in real samples with satisfactory results.

Author statement

Fatema Nazari: Formal analysis; Methodology; Software; Roles/Writing - original draft. Sayed Mehdi Ghoreishi: Data curation; Funding acquisition; Project administration; Resources; Supervision; Validation. Asma Khoobi: Conceptualization; Investigation; Validation; Visualization; Writing - review & editing.

Acknowledgements

The authors are grateful to University of Kashan for supporting this work by Grant No. (211037-40).

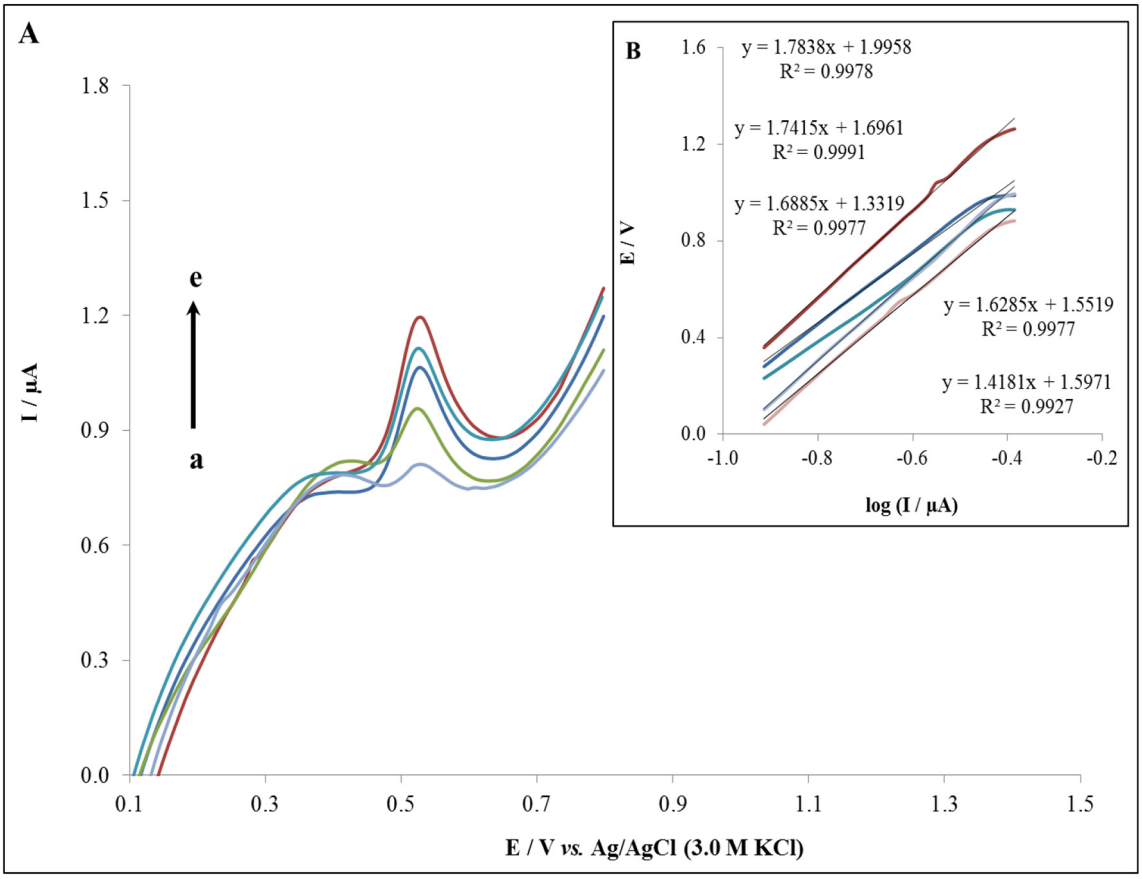

Fig. 14. (A) Linear sweep voltammograms of Fe_3O_4/Ch/CPE in 0.2 M phosphate buffer (pH = 2.0) containing 0.47, 0.64, 0.78, 0.97, and 1.15 μM of GA (from inner to outer) at a sweep rate of 130.0 mV s^{-1} and (B) Tafel plot derived from linear sweep voltammograms.

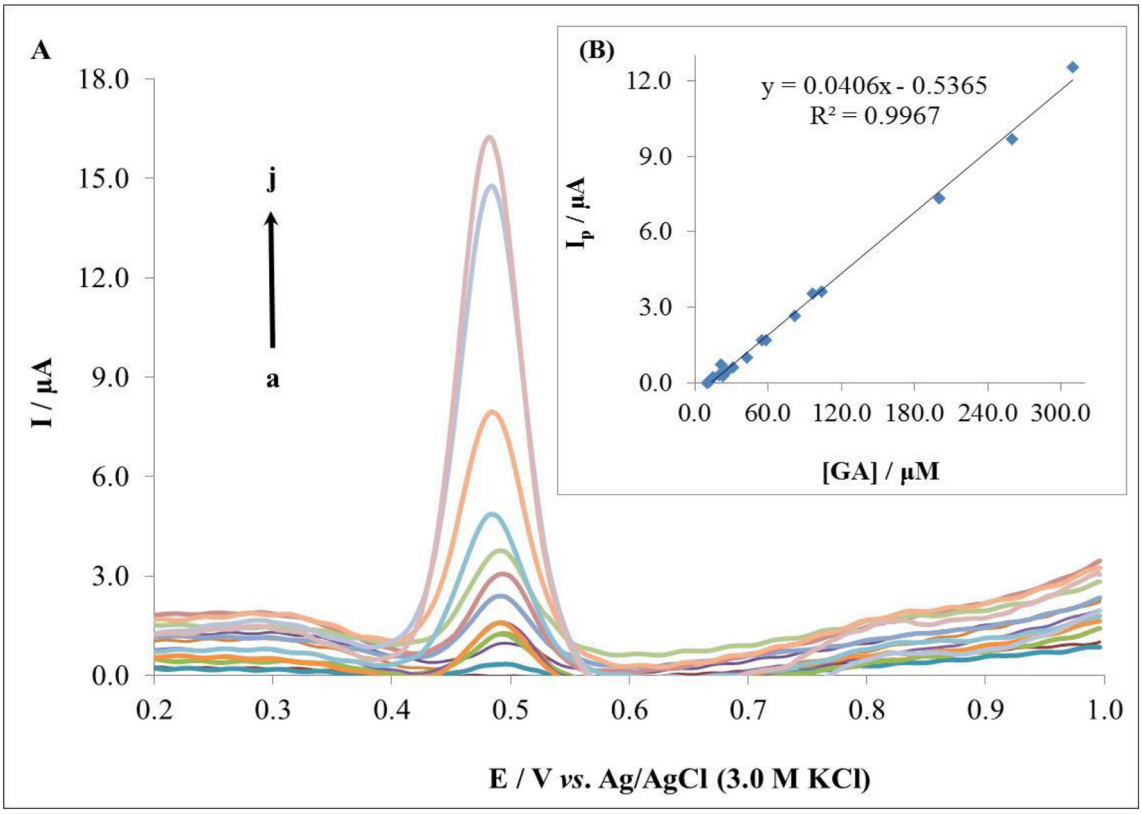

Fig. 15. DPV of Fe_3O_4/Ch/CPE in a phosphate buffer (pH = 2.0), containing different concentrations of GA. a to j correspond to: 1.0–300.0 μM of GA (A), plot of the catalytic peak current as a function of GA concentration (B).

Table 5
Comparison of the efficiency of some electrochemical techniques in the determination of GA.

Technique	Electrode material	Linear range (μM)	Detection limit (μM)	Reference
DPV	WCrGO/GCE	10–100	3.1	Stankovic et al. [23]
DPV	PEI-rGO/GCE	1–100	0.7	Luo et al. [24]
ASV	PEP/GCE	1–20	0.663	Refat and Newair [25]
SWV	PVA/GCE	1.6–49	0.495	Khan and Goh [26]
DPV	PmPD/Pal-IL	1–300	0.28	Wang et al. [27]
AMP	Bi-MWCNT/MCPE	1–100	0.16	Madhusudhana et al. [28]
DPV	IONPs/CPE	0.5–300.0	0.0121	This work

Abbreviations: WCrGO/GCE: wolfram carbide-doped reduced grapheme oxide/glassy carbon electrode; PEI-rGO: polyethyleneimine-functionalized graphene oxide; PEP: polyepinephrine; PVA: polyvinyl alcohol; PmPD/Pal-IL: poly(*m*-phenylenediamine)/palygorskite-ionic liquid; Bi-MWCNT/MCPE: bismuth nanoparticles decorated multi-wall-carbon-nanotubes modified carbon paste electrode; ASV: Anodic stripping voltammetry; SWV: square wave voltammetry; AMP: amperometry.

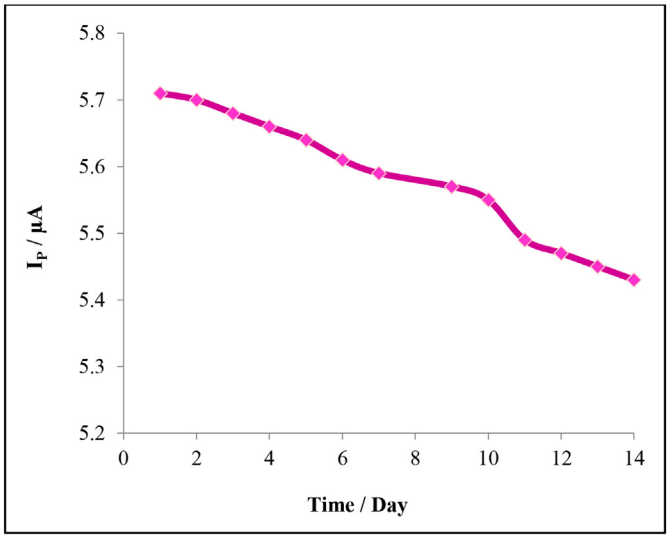

Fig. 16. Plot of stability of the modified electrode in 0.2 M phosphate (pH = 2.0), containing of 100.0 μM GA for a 2-week period.

Table 6
Influence of some interference substances in determination of GA at the surface of Fe_3O_4/Ch/CPE.

Interferences substance	Tolerance limit ($W_{Substance}/W_{GA}$)
NH_4^+, K^+, Na^+	500.0
NO_3^-, I^-, CO_3^{2-}, Cl^-, Br^-	500.0
L-tyrosin	200.0

Table 7
Determination of GA in green tea.

Sample	GA added (μM)	GA found (μM)	Recovery%
1	0.00	8.43	–
2	10.0	19.67	112.8
3	20.0	28.01	98.4
4	30.0	36.35	107.0

References

[1] Ç.C. Koçak, Ş.U. Karabiberoğlu, Z. Dursun, Highly sensitive determination of gallic acid on poly (l-methionine)-carbon nanotube composite electrode, J. Electroanal. Chem. 853 (2019) 113552.
[2] J. Tashkhourian, S.F. Nami-Ana, A sensitive electrochemical sensor for determination of gallic acid based on SiO_2 nanoparticle modified carbon paste electrode, Mater. Sci. Eng., C 52 (2015) 103–110.
[3] H.-M. Chen, Y.-C. Wua, Y.-C. Chia, F.-R. Chang, H.K. Hsu, Y.-C. Hsieh, C. C-Chen, S.-S. Yuan, Gallic acid, a major component of *Toona sinensis* leaf extracts, contains a ROS-mediated anti-cancer activity in human prostate cancer cells, Cancer Lett. 286 (2009) 161–171.
[4] B.R. You, W.H. Park, Gallic acid-induced lung cancer cell death is related to glutathione depletion as well as reactive oxygen species increase, Toxicol. in Vitro 24 (2010) 1356–1362.
[5] I. Mudnic, D. Modun, V. Rastija, J. Vukovic, I. Brizic, V. Katalinic, B. Kozina, M. Medic-Saric, M. Boban, Antioxidative and vasodilatory effects of phenolic acids in wine, Food Chem. 119 (2010) 1205–1210.
[6] B. Boye, E. Brillas, A. Buso, G. Farnia, C. Flox, M. Giomo, G. Sandon, Electrochemical removal of gallic acid from aqueous solutions, Electrochim. Acta 52 (2006) 256–262.
[7] B.B. Petković, D. Stanković, M. Milčić, S.P. Sovilj, D. Manojlović, Dinuclear copper (II) octaazamacrocyclic complex in a PVC coated GCE and graphite as a voltammetric sensor for determination of gallic acid and antioxidant capacity of wine samples, Talanta 13215 (2015) 513–519.
[8] K. Dhalwal, V.M. Shinde, Y.S. Biradar, K.R. Mahadik, Simultaneous quantification of bergenin, catechin, and gallic acid from Bergenia ciliata and Bergenia ligulata by using thin-layer chromatography, J. Food Compos. Anal. 21 (2008) 496–500.
[9] A.T. Vilian, J.Y. Song, Y.S. Lee, S.-K. Hwang, H.J. Kim, Y.-S. Jun, Y.S. Huh, Y.-K. Han, Salt-templated three-dimensional porous carbon for electrochemical determination of gallic acid, Biosens. Bioelectron. 117 (2018) 597–604.
[10] N. Al-Ansi, A. Salah, M. Bawa, S. Adlat, I. Yasmina, A. Abdallah, Bin Qi, 3D nitrogen-doped porous graphene aerogel as high-performance electrocatalyst for determination of gallic acid, Microchem. J. 155 (2020) 104706.
[11] N.S. Sangeetha, S.S. Narayanan, A novel bimediator amperometric sensor for electrocatalytic oxidation of gallic acid and reduction of hydrogen peroxide, Anal. Chim. Acta 828 (2014) 34–45.
[12] J. Tashkhourian, S.F. Nami-Ana, S. Hashemnia, M.R. Hormozi-Nezhad, Construction of a modified carbon paste electrode based on TiO_2 nanoparticles for the determination of gallic acid, J. Solid State Electrochem. 17 (2013) 157–165.
[13] M. Zaripour, V. Zare-Shahabadi, H. Jalali Jahromi, Application of ultrasonic-assisted inclusion complex formation with α-cyclodextrin for simultaneous spectrophotometric determination of gallic acid and vanillic acids in fruit samples, Spectrochim. Acta, Part A 222 (2019) 117197.
[14] M. Shaterian, A. Aghaei, M. Koohi, M. Teymouri, A. Mohammadi-Ganjgah, Synthesis, characterization and electrochemical sensing application of $CoFe_2O_4$/graphene magnetic nanocomposite for analysis of atenolol, Polyhedron 182 (2020), 114479.
[15] Y. Dang, Y. Zhai, L. Yang, Z. Peng, N. Chenga, Y. Zhou, Selective electrochemical detection of hydroquinone and catechol at a one-step synthesised pine needle-like nano-$CePO_4$ modified carbon paste electrode, RSC Adv. 6 (2016) 83994–84002.
[16] Y. Xie, X. Liu, Q. Chen, Synthesis and characterization of water-soluble chitosan derivate and its antibacterial activity, Carbohydr. Polym. 69 (2007) 142–147.
[17] H. Shagholani, S.M. Ghoreishi, S.H. Sharifi, Conversion of amine groups on chitosan-coated SPIONs into carbocyclic acid and investigation of its interaction with BSA in drug delivery systems, J. Drug. Deliv. Sci. Tec. 45 (2018) 373–377.
[18] A.M. Martins, G. Eng, S.G. Caridade, J.F. Mano, R.L. Reis, G. Vunjak-Novakovic, Electrically conductive chitosan/carbon scaffolds for cardiac tissue engineering, Biomacromolecules 15 (2014) 635–643.
[19] J.B. Marroquina, K.Y. Rhee, S.J. Park, Chitosan nanocomposite films: enhanced electrical conductivity, thermal stability, and mechanical properties, Carbohydr. Polym. 92 (2013) 1783–1791.
[20] R.G. Brereton, Applied Chemometrics for Scientists, John Wiley & Sons, Ltd, 2007.
[21] H. Shagholani, S.M. Ghoreishi, M. Mousazadeh, Improvement of interaction between PVA and chitosan via magnetite nanoparticles for drug delivery application, Int. J. Biol. Macromol. 78 (2015) 130–136.
[22] A.J. Bard, L.R. Faulkner, Electrochemical Methods, Fundamentals and Applications, Wiley, New York, 2001.
[23] D.M. Stankovic, M. Ognajanovic, F. Martin, L. Svroc, J.F.M.L. Mariano, B. Antic, Design of titanium nitride and wolfram carbide-doped RGO/GC electrodes for determination of gallic acid, Anal. Biochem. 539 (2017) 104–112.
[24] J.H. Luo, B.L. Li, N.B. Li, H.Q. Luo, Sensitive detection of gallic acid based on polyethyleneimine-functionalized grapheme modified glassy carbon electrode, Sensors Actuators B Chem. 186 (2013) 84–89.
[25] A.H. Refat, E.F. Newair, Adsorptive stripping voltammetric determination of gallic acid using an electrochemical sensor based on polyepinephrine/glassy carbon

electrode and its determination in black tea sample, J. Electroanal. Chem. 704 (2013) 32–37.
[26] S. Khan, J.K. Goh, Development of polymer-based chemical sensor to study the impact of polymer concentration and freeze-thaw cycle on the detection of gallic acid, Int. J. Electrochem. Sci. 15 (2020) 2307–2325.
[27] X. Wang, W. Tan, Y. Wang, D. Wu, Y. Kong, Electrosynthesis of poly(m-phenylenediamine) on the nanocomposites of palygorskite and ionic liquid for electrocatalytic sensing of gallic acid, Sensors & Actuators: B. Chemical 284 (2019) 63–72.
[28] Madhusudhana, G. Manasa, A.K. Bhakta, Z. Mekhalif, R.J. Mascarenhas, Bismuth-nanoparticles decorated multi-wall-carbon-nanotubes cast-coated on carbon paste electrode; an electrochemical sensor for sensitivedetermination of gallic acid at neutral pH, Materials Science for Energy Technologies 3 (2020) 174–182.